Available online at www.sciencedirect.com
SCIENCE DIRECT®
International Journal of Heat and Mass Transfer 47 (2004) 1383–1389
International Journal of HEAT and MASS TRANSFER
www.elsevier.com/locate/ijhmt

Self-similar solidification: morphological stability of the regime

D.V. Alexandrov *

Department of Mathematical Physics, Urals State University, Lenin Avenue 51, Ekaterinburg 620083, Russia

Received 15 April 2003; received in revised form 26 June 2003

Abstract

The morphological instability analysis is carried out for non-stationary solidification of a binary melt. We demonstrate that both the morphological and dynamic neutral stability curves coincide. The neutral stability curve for morphological perturbations does not intersect the self-similar branch of solutions for solidification, that is, the morphological instability does not cause the mushy zone origination whereas the constitutional supercooling arising ahead of the stable planar front solidifying in self-similar manner is a reasonable criterion for the mushy region incipience. The theory under consideration is in a good agreement with experimental and numerical studies carried out by Huppert and Worster.

1. Introduction

It is well-known that the planar solid–liquid interface may be destroyed by small perturbations in the case of steady-state solidification scenario [1]. There are variety of situations when crystallization processes proceed in unsteady state manner. To establish a condition between physical (alloy properties) and operating parameters describing a transition from the planar to mushy solidification scenario it is required to carry out a morphological instability analysis for non-stationary solidification. One of the known non-stationary processes is the self-similar regime when solidification front is far from the walls of an ingot mold and it is not sensitive to own prehistory, that is, a relation between the spatial coordinate and the time of solidification is constant. The key idea of the present paper is to study a possibility of planar solidification front break-down due to the constitutional supercooling and/or small morphological perturbations within a framework of the self-similar crystallization regime. Coriell with co-authors have made progress in this matter [2]. They have carried out a dynamic instability analysis for solidification and melting. In other words, their study is devoted to the instability evolution with zero wavenumber, that is, the front is perturbed as a whole and its shape is always planar. Such a situation practically corresponds to perturbations in the self-similar rate of solidification.

However, instabilities may be caused by constitutional supercooling which leads to favorable conditions for the growth of occasional solid ridges into the supercooled melt. In this case, the plane morphology is destroyed and the solid–liquid interface may be morphologically unstable. Moreover, solid phase in the form of newly born crystals may grow in ambient supercooled zone ahead of the front. Taking into account both of these factors, we characterize a mushy region as a zone of mixed phases between pure solid and liquid. At present, there are a lot of papers describing solidification and melting with a mushy layer. So, for example, self-similar behaviour of the mush was studied by Huppert and Worster [3], Worster [4], Feltham and Worster [5].

From our point of view, in order to study a transition from the planar to mushy solidification scenario it is required to take into consideration an influence of a constitutional supercooling on instability behaviour of crystallization. Contrary to Ref. [2] and other papers on this subject where instability analysis was made in some limiting cases (see Discussion in Ref. [2]), this study is connected with the morphological instability analysis for any wavenumbers of perturbations. How to construct a

* Tel.: +7-343-2-557541; fax: +7-343-2-557401.
E-mail address: dmitri.alexandrov@usu.ru (D.V. Alexandrov).

0017-9310/$ - see front matter © 2003 Elsevier Ltd. All rights reserved.
doi:10.1016/j.ijheatmasstransfer.2003.08.009

Nomenclature

C_L	solute concentration in the liquid
C'_L	perturbation in the liquid phase concentration
C_{LI}	solute concentration at the front
C_{LS}	self-similar concentration in the liquid
$C_{L\infty}$	solute concentration at infinity
C_S	concentration in the solid
C'_S	perturbation in the solid phase concentration
C_{SS}	self-similar concentration in the solid
C_W	concentration at the wall $x = 0$
D_L	diffusion coefficient in the liquid
D_S	diffusion coefficient in the solid
k	equilibrium segregation coefficient
K	front curvature
K_L	thermal conductivity in the liquid
K_S	thermal conductivity in the solid
L_V	latent heat parameter
m	liquidus slope
t	time
T_L	temperature in the liquid
T_{LS}	self-similar temperature in the liquid
T'_L	perturbation in the liquid phase temperature
$T_{L\infty}$	temperature at infinity
T_M	phase transition temperature for pure matter
T_S	temperature in the solid
T'_S	perturbation in the solid phase temperature
T_{SS}	self-similar temperature in the solid
T_W	temperature at the wall $x = 0$
x	spatial coordinate parallel to the direction of solidification
X	front position
y	spatial coordinate perpendicular to the direction of solidification

Greek symbols

Γ	surface tension
Δ	Laplacian
$\eta = x/\sqrt{t} - \lambda$	self-similar coordinate
κ_L	thermal diffusivity in the liquid
κ_S	thermal diffusivity in the solid
λ	parabolic growth rate constant
$\Sigma = X/\sqrt{t} - \lambda$	self-similar front position
$\tau = \sqrt{t}$	self-similar variable of time

perturbation theory in self-similar solidification conditions for binary melts is a subject of our subsequent theory.

2. Self-similar solidification

We treat a unidirectional solidification of a binary melt along x-axis. The temperatures T_S in the solid and T_L in the liquid, and the melt concentrations C_S and C_L in these phases are governed by the following equations:

$$\frac{\partial T_S}{\partial t} = \kappa_S \Delta_{xy} T_S, \quad \frac{\partial C_S}{\partial t} = D_S \Delta_{xy} C_S, \quad 0 < x < X(t,y), \tag{1}$$

$$\frac{\partial T_L}{\partial t} = \kappa_L \Delta_{xy} T_L, \quad \frac{\partial C_L}{\partial t} = D_L \Delta_{xy} C_L, \quad x > X(t,y), \tag{2}$$

where κ_S and κ_L are the thermal diffusivities in the solid and liquid phases, D_S and D_L are the diffusion coefficients; all of which are assumed constant in each phase, $\Delta = \partial^2/\partial x^2 + \partial^2/\partial y^2$ is the Laplacian. In the case of self-similar regime with a planar front nothing depends on the spatial coordinate y directed perpendicular to solidification direction.

Further, we make the assumption that the front, $x = X(t,y)$, is close to equilibrium, that is,

$$T_S = T_L = T_M + mC_L + \Gamma T_M K, \quad x = X(t,y). \tag{3}$$

Here m and T_M stand for the liquidus slope and the phase transition temperature for pure matter, Γ is the surface tension. In Section 3, we consider linear instability analysis which implies that the front shape is nearly planar due to small non-planar perturbations. In this case, the front curvature, K, may be also written in the linear form, that is, $K = \partial^2 X/\partial y^2$.

Heat and solute must be conserved at the front

$$K_S \frac{\partial T_S}{\partial x} - K_L \frac{\partial T_L}{\partial x} = L_V \frac{\partial X}{\partial t}, \quad x = X(t,y), \tag{4}$$

$$(1-k)C_L \frac{\partial X}{\partial t} + D_L \frac{\partial C_L}{\partial x} - D_S \frac{\partial C_S}{\partial x} = 0, \quad x = X(t,y), \quad C_S = kC_L, \tag{5}$$

where K_S and K_L are the thermal conductivities in the solid and liquid, L_V is the latent heat parameter, and k is the equilibrium segregation coefficient.

Finally, the temperature and concentration fields will be regarded as known at $x = 0$ and $x \to \infty$, that is,

$$T_S = T_W, \quad C_S = C_W, \quad x = 0, \tag{6}$$

$$T_L \to T_{L\infty}, \quad C_L \to C_{L\infty}, \quad x \to \infty. \tag{7}$$

The second boundary condition in Eq. (6) implies that the process with the constant concentration $C_{L\infty}$ in the

melt starts from the wall $x = 0$, that is, $X = 0$ at the initial time and the solid phase concentration, $C_S = C_W$ at $x = 0$, produced by crystallization will be $C_W = kC_{L\infty}$ near the wall $x = 0$. Strictly speaking, the concentration C_W is not constant with time. However, a relaxation time of the diffusion field in solids is extremely large and, as a consequence, C_W as well as the solid phase concentration profile will be changed over an extremely long period of time.

Now, let us choose the following self-similar parameters

$$\eta = \frac{x}{\sqrt{t}} - \lambda, \quad \Sigma(y,\tau) = \frac{X(y,t)}{\sqrt{t}} - \lambda, \quad \tau = \sqrt{t}. \tag{8}$$

If the solidification regime can be treated as established, the planar front has the position $X = \lambda\sqrt{t}$, that is, $\Sigma = 0$. In this case, all functions depend only on self-similar variable η. Thus, the parabolic growth rate constant λ determines the self-similar solidification rate $\mathrm{d}X/\mathrm{d}t = \lambda/2\sqrt{t}$, whereas time τ characterizes deviations from self-similarity.

Further, let us write down the set (1), (2) supplemented by the boundary conditions (3)–(7) in self-similar variables (8). The result is

$$\begin{aligned}
&\frac{\tau}{2}\frac{\partial T_S}{\partial \tau} = \frac{1}{2}(\eta+\lambda)\frac{\partial T_S}{\partial \eta} + \kappa_S\left(\frac{\partial^2 T_S}{\partial \eta^2} + \tau^2\frac{\partial^2 T_S}{\partial y^2}\right),\\
&\quad -\lambda < \eta < \Sigma(y,\tau),\\
&\frac{\tau}{2}\frac{\partial C_S}{\partial \tau} = \frac{1}{2}(\eta+\lambda)\frac{\partial C_S}{\partial \eta} + D_S\left(\frac{\partial^2 C_S}{\partial \eta^2} + \tau^2\frac{\partial^2 C_S}{\partial y^2}\right),\\
&\quad -\lambda < \eta < \Sigma(y,\tau),\\
&\frac{\tau}{2}\frac{\partial T_L}{\partial \tau} = \frac{1}{2}(\eta+\lambda)\frac{\partial T_L}{\partial \eta} + \kappa_L\left(\frac{\partial^2 T_L}{\partial \eta^2} + \tau^2\frac{\partial^2 T_L}{\partial y^2}\right),\\
&\quad \eta > \Sigma(y,\tau),\\
&\frac{\tau}{2}\frac{\partial C_L}{\partial \tau} = \frac{1}{2}(\eta+\lambda)\frac{\partial C_L}{\partial \eta} + D_L\left(\frac{\partial^2 C_L}{\partial \eta^2} + \tau^2\frac{\partial^2 C_L}{\partial y^2}\right),\\
&\quad \eta > \Sigma(y,\tau).
\end{aligned} \tag{9}$$

$$T_L = T_S = T_M + mC_L + \Gamma T_M \tau\frac{\partial^2 \Sigma(y,\tau)}{\partial y^2}, \quad \eta = \Sigma(y,\tau), \tag{10}$$

$$\frac{L_V}{2}\left[\Sigma(y,\tau) + \lambda + \tau\frac{\partial \Sigma(y,\tau)}{\partial \tau}\right] = K_S\frac{\partial T_S}{\partial \eta} - K_L\frac{\partial T_L}{\partial \eta}, \quad \eta = \Sigma(y,\tau), \tag{11}$$

$$\begin{aligned}
&\frac{(1-k)C_L}{2}\left[\Sigma(y,\tau) + \lambda + \tau\frac{\partial \Sigma(y,\tau)}{\partial \tau}\right]\\
&\quad + D_L\frac{\partial C_L}{\partial \eta} - D_S\frac{\partial C_S}{\partial \eta} = 0,\\
&C_S = kC_L, \quad \eta = \Sigma(y,\tau).
\end{aligned} \tag{12}$$

Now, conditions (6) and (7) are valid at $\eta = -\lambda$ and $\eta \to \infty$, respectively.

Self-similar solutions $T_{SS}(\eta)$, $C_{SS}(\eta)$, $T_{LS}(\eta)$, $C_{LS}(\eta)$ of the set above have the forms

$$\begin{aligned}
&T_{SS}(\eta) = T_W + (T_M + mC_{LI} - T_W)\frac{\mathrm{erf}((\eta+\lambda)/\sqrt{4\kappa_S})}{\mathrm{erf}(\lambda/\sqrt{4\kappa_S})},\\
&\quad -\lambda < \eta < 0,\\
&C_{SS}(\eta) = C_W + (kC_{LI} - C_W)\frac{\mathrm{erf}((\eta+\lambda)/\sqrt{4D_S})}{\mathrm{erf}(\lambda/\sqrt{4D_S})},\\
&\quad -\lambda < \eta < 0,\\
&T_{LS}(\eta) = T_{L\infty} + (T_M + mC_{LI} - T_{L\infty})\frac{\mathrm{erfc}((\eta+\lambda)/\sqrt{4\kappa_L})}{\mathrm{erfc}(\lambda/\sqrt{4\kappa_L})},\\
&\quad \eta > 0,\\
&C_{LS}(\eta) = C_{L\infty} + (C_{LI} - C_{L\infty})\frac{\mathrm{erfc}((\eta+\lambda)/\sqrt{4D_L})}{\mathrm{erfc}(\lambda/\sqrt{4D_L})},\\
&\quad \eta > 0.
\end{aligned} \tag{13}$$

The distribution $C_{SS}(\eta)$ above is nearly linear function due to small values of D_S. Physically it means that the process is self-similar and the concentration at the front is practically unchanged.

Substitution of expressions (13) in the boundary conditions (10)–(12) at $\eta = 0$ gives two relations connecting the parabolic growth rate constant λ and the impurity concentration C_{LI} at the planar front dependent on physical and operating parameters. Coriell with co-authors have deduced similar relations in infinite domain (see Ref. [6]) and considered some limiting situations to express λ and C_{LI} in approximate forms. Let us write down only the final result in terms of T_W and C_{LI}:

$$\begin{aligned}
&T_W(\lambda)\\
&\quad = T_M + mC_{LI} - \frac{\lambda L_V\sqrt{\pi\kappa_S}\mathrm{erf}(\lambda/\sqrt{4\kappa_S})}{2K_S\exp[-\lambda^2/4\kappa_S]}\\
&\quad + \frac{K_L\sqrt{\kappa_S}(T_M + mC_{LI} - T_{L\infty})\exp[-\lambda^2/4\kappa_L]\mathrm{erf}(\lambda/\sqrt{4\kappa_S})}{K_S\sqrt{\kappa_L}\exp[-\lambda^2/4\kappa_S]\mathrm{erfc}(\lambda/\sqrt{4\kappa_L})},
\end{aligned} \tag{14}$$

$$\begin{aligned}
C_{LI}(\lambda) = C_{L\infty}\Big(&\sqrt{D_L}\exp[-\lambda^2/4D_L]\mathrm{erf}(\lambda/\sqrt{4D_S})\\
&+ k\sqrt{D_S}\exp[-\lambda^2/4D_S]\mathrm{erfc}(\lambda/\sqrt{4D_L})\Big)\Big/Z(\lambda),
\end{aligned} \tag{15}$$

where

$$\begin{aligned}
Z(\lambda) = &\sqrt{D_L}\exp[-\lambda^2/4D_L]\mathrm{erf}(\lambda/\sqrt{4D_S})\\
&+ k\sqrt{D_S}\exp[-\lambda^2/4D_S]\mathrm{erfc}(\lambda/\sqrt{4D_L})\\
&- (1-k)\lambda\sqrt{\pi}\mathrm{erf}(\lambda/\sqrt{4D_S})\mathrm{erfc}(\lambda/\sqrt{4D_L})/2 > 0,
\end{aligned}$$

$C_W = kC_{L\infty}$.

Self-similar solidification scenario may be destroyed, for example, by the constitutional supercooling which appears if the concentration gradient exceeds the temperature one at the front, that is,

$$m\frac{\mathrm{d}C_{\mathrm{LS}}}{\mathrm{d}\eta} > \frac{\mathrm{d}T_{\mathrm{LS}}}{\mathrm{d}\eta}, \quad \eta = 0. \tag{16}$$

Substituting the self-similar distributions (13) in condition (16), we get the condition which describes existence of the constitutional supercooling in the self-similar case

$$m\frac{(C_{\mathrm{LI}} - C_{\mathrm{L}\infty})}{\sqrt{D_{\mathrm{L}}}}U\left(\frac{\lambda}{\sqrt{4D_{\mathrm{L}}}}\right) - \frac{T_{\mathrm{M}} + mC_{\mathrm{LI}} - T_{\mathrm{L}\infty}}{\sqrt{\kappa_{\mathrm{L}}}}U\left(\frac{\lambda}{\sqrt{4\kappa_{\mathrm{L}}}}\right) < 0, \tag{17}$$

$U(\xi) = \exp[-\xi^2]/\mathrm{erfc}(\xi)$.

Let us now pay our attention to the linear instability analysis which strongly determines scenario of morphological evolution.

3. Linear analysis of morphological instability

Let us perturb the self-similar temperature and concentration profiles (13) as well as the front position $\Sigma = 0$ as follows:

$$T'_{\mathrm{S}} = T_S - T_{\mathrm{SS}}, \quad C'_{\mathrm{S}} = C_{\mathrm{S}} - C_{\mathrm{SS}}, \quad T'_{\mathrm{L}} = T_{\mathrm{L}} - T_{\mathrm{LS}}, \quad C'_{\mathrm{L}} = C_{\mathrm{L}} - C_{\mathrm{LS}}, \quad \Sigma = \Sigma'.$$

Practically it means, that the self-similar temperature and concentration profiles as well as the front velocity and position get the time and y-dependent small additions due to different perturbations which always exist in the system (for example, small oscillations of the temperature field, small mechanical oscillations of the ingot mold and the like).

Substituting these perturbations in Eq. (9), expanding boundary conditions (10)–(12) in Teylor's series at point $\eta = 0$, and taking into account only linear terms in perturbations, we come to

$$\frac{\tau}{2}\frac{\partial T'_{\mathrm{L}}}{\partial \tau} = \frac{1}{2}(\eta + \lambda)\frac{\partial T'_{\mathrm{L}}}{\partial \eta} + \kappa_{\mathrm{L}}\left(\frac{\partial^2 T'_{\mathrm{L}}}{\partial \eta^2} + \tau^2\frac{\partial^2 T'_{\mathrm{L}}}{\partial y^2}\right), \quad \eta > \Sigma, \tag{18}$$

with similar forms for the perturbations T'_{S}, C'_{S} and C'_{L} and

$$T'_{\mathrm{S}} - T'_{\mathrm{L}} + H_1(\lambda)\Sigma' = 0, \quad H_1(\lambda) = \frac{\mathrm{d}T_{\mathrm{SS}}}{\mathrm{d}\eta} - \frac{\mathrm{d}T_{\mathrm{LS}}}{\mathrm{d}\eta}, \quad \eta = 0, \tag{19}$$

$$T'_{\mathrm{L}} - mC'_{\mathrm{L}} + H_2(\lambda)\Sigma' - \Gamma T_{\mathrm{M}}\tau\frac{\partial^2 \Sigma'}{\partial y^2} = 0, \quad \eta = 0, \tag{20}$$

$$K_{\mathrm{S}}\frac{\partial T'_{\mathrm{S}}}{\partial \eta} - K_{\mathrm{L}}\frac{\partial T'_{\mathrm{L}}}{\partial \eta} + H_3(\lambda)\Sigma' - \frac{L_V}{2}\tau\frac{\partial \Sigma'}{\partial \tau} = 0, \quad \eta = 0, \tag{21}$$

$$\frac{1-k}{2}\lambda C'_{\mathrm{L}} + D_{\mathrm{L}}\frac{\partial C'_{\mathrm{L}}}{\partial \eta} - D_{\mathrm{S}}\frac{\partial C'_{\mathrm{S}}}{\partial \eta} + H_4(\lambda)\Sigma' + \frac{1-k}{2}C_{\mathrm{LS}}\tau\frac{\partial \Sigma'}{\partial \tau} = 0, \quad \eta = 0, \tag{22}$$

$$C'_{\mathrm{S}} - kC'_{\mathrm{L}} + H_5\Sigma' = 0, \quad \eta = 0, \tag{23}$$

where the following notations are introduced

$$H_2(\lambda) = \frac{\mathrm{d}T_{\mathrm{LS}}}{\mathrm{d}\eta} - m\frac{\mathrm{d}C_{\mathrm{LS}}}{\mathrm{d}\eta},$$

$$H_3(\lambda) = K_{\mathrm{S}}\frac{\mathrm{d}^2 T_{\mathrm{SS}}}{\mathrm{d}\eta^2} - K_{\mathrm{L}}\frac{\mathrm{d}^2 T_{\mathrm{LS}}}{\mathrm{d}\eta^2} - \frac{L_V}{2}, \quad \eta = 0,$$

$$H_4(\lambda) = D_{\mathrm{L}}\frac{\mathrm{d}^2 C_{\mathrm{LS}}}{\mathrm{d}\eta^2} + \frac{1-k}{2}C_{\mathrm{LS}} + \frac{1-k}{2}\lambda\frac{\mathrm{d}C_{\mathrm{LS}}}{\mathrm{d}\eta} - D_{\mathrm{S}}\frac{\mathrm{d}^2 C_{\mathrm{SS}}}{\mathrm{d}\eta^2}, \quad \eta = 0,$$

$$H_5 = \frac{\mathrm{d}C_{\mathrm{SS}}}{\mathrm{d}\eta} - k\frac{\mathrm{d}C_{\mathrm{LS}}}{\mathrm{d}\eta}, \quad \eta = 0.$$

Here, for the sake of simplicity, we do not substitute the self-similar distributions (13). With this object in view, we write down only the equation for the temperature perturbations in the liquid.

Let us pay our attention to the neutral stability curve in a plane of any operating parameters for morphological perturbations. In this case, nothing depends on τ. As is seen from Eq. (18) for the liquid temperature perturbations and analogous ones for T'_{S}, C'_{L} and C'_{S} as well as from the boundary conditions above at $\eta = 0$, all perturbations may be dependent only on y as linear functions, i.e. $T'_{\mathrm{L}} = T_{\mathrm{L}1}(\eta) + T_{\mathrm{L}2}(\eta)y$, $T'_{\mathrm{S}} = T_{\mathrm{S}1}(\eta) + T_{\mathrm{S}2}(\eta)y$, $C'_{\mathrm{L}} = C_{\mathrm{L}1}(\eta) + C_{\mathrm{L}2}(\eta)y$ and $C'_{\mathrm{S}} = C_{\mathrm{S}1}(\eta) + C_{\mathrm{S}2}(\eta)y$. Further, substituting these functions in Eq. (18) and analogous ones for T'_{S}, C'_{L} and C'_{S}, we obtain

$$\frac{1}{2}(\eta + \lambda)\frac{\mathrm{d}T'_{\mathrm{L}}}{\mathrm{d}\eta} + \kappa_{\mathrm{L}}\frac{\mathrm{d}^2 T'_{\mathrm{L}}}{\mathrm{d}\eta^2} = 0,$$

$$\frac{1}{2}(\eta + \lambda)\frac{\mathrm{d}T'_{\mathrm{S}}}{\mathrm{d}\eta} + \kappa_{\mathrm{S}}\frac{\mathrm{d}^2 T'_{\mathrm{S}}}{\mathrm{d}\eta^2} = 0, \tag{24}$$

$$\frac{1}{2}(\eta + \lambda)\frac{\mathrm{d}C'_{\mathrm{L}}}{\mathrm{d}\eta} + D_{\mathrm{L}}\frac{\mathrm{d}^2 C'_{\mathrm{L}}}{\mathrm{d}\eta^2} = 0,$$

$$\frac{1}{2}(\eta + \lambda)\frac{\mathrm{d}C'_{\mathrm{S}}}{\mathrm{d}\eta} + D_{\mathrm{S}}\frac{\mathrm{d}^2 C'_{\mathrm{S}}}{\mathrm{d}\eta^2} = 0. \tag{25}$$

Taking into consideration boundary conditions (6) and (7) that imply $T'_{\mathrm{S}} \to 0$ and $C'_{\mathrm{S}} \to 0$ as $\eta \to -\lambda$; $T'_{\mathrm{L}} \to 0$ and $C'_{\mathrm{L}} \to 0$ as $\eta \to \infty$, we write down solutions of Eqs. (24) and (25) at the neutral stability curve in the form

$$T'_{\mathrm{S}} = h_1\mathrm{erf}\left(\frac{\eta + \lambda}{\sqrt{4\kappa_{\mathrm{S}}}}\right), \quad C'_{\mathrm{S}} = h_2\mathrm{erf}\left(\frac{\eta + \lambda}{\sqrt{4D_{\mathrm{S}}}}\right), \tag{26}$$

$$T'_{\mathrm{L}} = h_3 \mathrm{erfc}\left(\frac{\eta+\lambda}{\sqrt{4\kappa_{\mathrm{L}}}}\right), \quad C'_{\mathrm{L}} = h_4 \mathrm{erfc}\left(\frac{\eta+\lambda}{\sqrt{4D_{\mathrm{L}}}}\right), \tag{27}$$

$$h_1 = h_{11} + h_{12}y, \quad h_2 = h_{21} + h_{22}y,$$
$$h_3 = h_{31} + h_{32}y, \quad h_4 = h_{41} + h_{42}y,$$

where h_1, h_2, h_3 and h_4 stand for the perturbation amplitudes and h_{11}, h_{12}, h_{21}, h_{22}, h_{31}, h_{32}, h_{41} and h_{42} are arbitrary constants. Let us especially emphasize here that solutions (26) and (27) satisfy to the boundary conditions (19)–(23) at the neutral stability curve (nothing depends on τ) only if

$$\Sigma' = h_5 = \Sigma_1 + \Sigma_2 y, \tag{28}$$

where Σ_1 and Σ_2 are constants.

Now, solutions (26)–(28) supplemented by the boundary conditions (19)–(23) coincide with similar ones for dynamic perturbations at the neutral stability curve when nothing depends on y and τ (see also Ref. [2]). The difference is only that amplitudes h_i $(i = 1, 2, 3, 4, 5)$ are functions of y in the present case of morphological instability analysis whereas these amplitudes are constants in the case of dynamic instability analysis. The latter circumstance is not principal due to the following procedure.

Substituting perturbations (26)–(28) into the boundary conditions (19)–(23), we obtain five linear equations in amplitudes h_1, h_2, h_3, h_4 and h_5. Equating to zero the determinant consisting of the amplitude coefficients, we come to the expression describing the neutral stability curve (thus, now nothing depends on the amplitudes h_i). However, we will not dwell on this point to save room. Expressing $T_{\mathrm{W}}(\lambda)$ from this equation and equating the result to the right hand side of relation (14), and keeping in mind relation (15) and the following one $C_{\mathrm{W}} = kC_{\mathrm{L}\infty}$, one can get a point of intersection of the neutral stability curve and the self-similar solution (of course, if such a point exists). Performing a lot of cumbersome and tedious calculations, we write down this equation in the final form

$$\begin{aligned}
&\left[k\mathrm{erfc}\left(\frac{\lambda}{\sqrt{4D_{\mathrm{L}}}}\right)\left(\sqrt{\frac{D_{\mathrm{S}}}{\pi}}\mathrm{e}^{-\lambda^2/4D_{\mathrm{S}}} + \frac{\lambda}{2}\mathrm{erf}\left(\frac{\lambda}{\sqrt{4D_{\mathrm{S}}}}\right)\right)\right.\\
&\left.+\mathrm{erf}\left(\frac{\lambda}{\sqrt{4D_{\mathrm{S}}}}\right)\sqrt{\frac{D_{\mathrm{L}}}{\pi}}\left(\mathrm{e}^{-\lambda^2/4D_{\mathrm{L}}} - \frac{\lambda\sqrt{\pi}}{2\sqrt{D_{\mathrm{L}}}}\mathrm{erfc}\left(\frac{\lambda}{\sqrt{4D_{\mathrm{L}}}}\right)\right)\right]\\
&\times\left[K_{\mathrm{L}}(mC_{\mathrm{LI}} - T_{\mathrm{L}\infty})\mathrm{e}^{-\lambda^2/4\kappa_{\mathrm{L}}}\left[\left(\frac{\lambda\sqrt{\pi}}{2\sqrt{\kappa_{\mathrm{L}}}}\mathrm{erfc}\left(\frac{\lambda}{\sqrt{4\kappa_{\mathrm{L}}}}\right)\right.\right.\right.\\
&\left.\left.-\mathrm{e}^{-\lambda^2/4\kappa_{\mathrm{L}}}\right)\mathrm{erf}\left(\frac{\lambda}{\sqrt{4\kappa_{\mathrm{S}}}}\right)\Big/\left(\pi\kappa_{\mathrm{L}}\mathrm{erfc}\left(\frac{\lambda}{\sqrt{4\kappa_{\mathrm{L}}}}\right)\right)\right.\\
&\left.-\lambda\mathrm{erf}\left(\frac{\lambda}{\sqrt{4\kappa_{\mathrm{S}}}}\right)\Big/\left(2\kappa_{\mathrm{S}}\sqrt{\pi\kappa_{\mathrm{L}}}\right) - \mathrm{e}^{-\lambda^2/4\kappa_{\mathrm{S}}}/\left(\pi\sqrt{\kappa_{\mathrm{L}}\kappa_{\mathrm{S}}}\right)\right]\\
&\left.+T_1(\lambda)\right] = m\frac{T_2(\lambda)(1-k)}{2Z(\lambda)}\mathrm{erf}\left(\frac{\lambda}{\sqrt{4D_{\mathrm{S}}}}\right)\mathrm{erfc}\left(\frac{\lambda}{\sqrt{4D_{\mathrm{L}}}}\right)\\
&\times C_{\mathrm{L}\infty}\left[\sqrt{D_{\mathrm{L}}}\mathrm{e}^{-\lambda^2/4D_{\mathrm{L}}}\left(\mathrm{erfc}\left(\frac{\lambda}{\sqrt{4D_{\mathrm{L}}}}\right) - \frac{\lambda}{\sqrt{\pi D_{\mathrm{L}}}}\mathrm{e}^{-\lambda^2/4D_{\mathrm{L}}}\right.\right.\\
&\left.\left.+\frac{\lambda^2}{2D_{\mathrm{L}}}\mathrm{erfc}\left(\frac{\lambda}{\sqrt{4D_{\mathrm{L}}}}\right)\right)\mathrm{erf}\left(\frac{\lambda}{\sqrt{4D_{\mathrm{S}}}}\right)\Big/\mathrm{erfc}\left(\frac{\lambda}{\sqrt{4D_{\mathrm{L}}}}\right)\right.\\
&\left.+k\sqrt{D_{\mathrm{S}}}\mathrm{erfc}\left(\frac{\lambda}{\sqrt{4D_{\mathrm{L}}}}\right)\mathrm{e}^{-\lambda^2/4D_{\mathrm{S}}}\right.\\
&\left.\times\left(1+\frac{\lambda^2}{2D_{\mathrm{S}}}+\lambda\mathrm{e}^{-\lambda^2/4D_{\mathrm{S}}}\Big/\left(\sqrt{\pi D_{\mathrm{S}}}\mathrm{erf}\left(\frac{\lambda}{\sqrt{4D_{\mathrm{S}}}}\right)\right)\right)\right],
\end{aligned} \tag{29}$$

where the following positive functions are introduced $(\lambda > 0)$

$$\begin{aligned}
T_1(\lambda) &= \frac{L_V}{4\kappa_{\mathrm{S}}}\mathrm{erfc}\left(\frac{\lambda}{\sqrt{4\kappa_{\mathrm{L}}}}\right)\left[(2\kappa_{\mathrm{S}}+\lambda^2)\mathrm{erf}\left(\frac{\lambda}{\sqrt{4\kappa_{\mathrm{S}}}}\right)\right.\\
&\left.+2\lambda\sqrt{\kappa_{\mathrm{S}}}\mathrm{e}^{-\lambda^2/4\kappa_{\mathrm{S}}}/\sqrt{\pi}\right],\\
T_2(\lambda) &= \frac{K_{\mathrm{L}}}{\sqrt{\pi\kappa_{\mathrm{L}}}}\mathrm{e}^{-\lambda^2/4\kappa_{\mathrm{L}}}\mathrm{erf}\left(\frac{\lambda}{\sqrt{4\kappa_{\mathrm{S}}}}\right)\\
&+\frac{K_{\mathrm{S}}}{\sqrt{\pi\kappa_{\mathrm{S}}}}\mathrm{e}^{-\lambda^2/4\kappa_{\mathrm{S}}}\mathrm{erfc}\left(\frac{\lambda}{\sqrt{4\kappa_{\mathrm{L}}}}\right),
\end{aligned}$$

and temperatures are measured from the melting point, that is, $T_{\mathrm{M}} = 0$.

Let us pay our attention to the case of positive λ. In this case, the function

$$f_1(x) \equiv x\sqrt{\pi}\mathrm{erfc}(x) - \mathrm{e}^{-x^2},$$

twice entering on the left hand side of Eq. (29) is always negative whereas the function

$$f_2(x) \equiv \mathrm{erfc}(x) - \frac{2x}{\sqrt{\pi}}\mathrm{e}^{-x^2} + 2x^2\mathrm{erfc}(x),$$

entering on the right is always positive. Since the liquidus slope in the present study is assumed negative [see Eq. (3)], it immediately follows that the left hand side of Eq. (29) is positive and the right one is negative for any $\lambda > 0$ and for any physical and operating parameters. This conclusion is strengthened by the numerical calculations of functions $f_1(x)$ and $f_2(x)$ as well as of Eq. (29). In other words, the neutral stability curve does not intersect the self-similar branch of solutions for solidification $(\lambda > 0)$, that is, a transition between morphologically stable and unstable regimes does not exist in this case. This result is strengthened by numerical calculations carried out in Ref. [2].

Further, setting $\lambda = 0$ in Eq. (29), it is easy to conclude that the latter becomes identity, that is, $\lambda = 0$ is the root and, therefore, it divides the stable and unstable regimes. Similar results were obtained in Ref. [2] for solidification in infinite domain. However, experiments [3] and [4] show that the mushy zone appears at certain

values of parameters. We demonstrate in Fig. 1 the parabolic growth rate constant $\lambda_1 \equiv \lambda/2\sqrt{D_L}$ as a function of the temperature $T_1 \equiv -T_W + mC_{L\infty}$ in accordance with the self-similar solutions (14) and (15). The calculations are carried out for the aqueous solution of sodium nitrate, $NaNO_3$, with $k = 0$ experimentally and numerically studied in Refs. [3] and [4]. Thermophysical properties of this solution are given in Table 1. Equating both sides of inequality (17) to each other, we plot in Fig. 1 the root (point A: $\lambda_{1A} \approx 0.1537$ and $T_{1A} \approx 1.77$) which divides the constitutional supercooling regime and the regime when supercooling is absent. The inequality (17) takes place if $\lambda_1 > \lambda_{1A}$ and is not valid in the opposite case. In other words, if $\lambda_1 > \lambda_{1A}$ the metastable supercooled zone exists while if $\lambda_1 < \lambda_{1A}$ solidification proceeds in accordance with the stable self-similar manner.

Experiments and computations performed in Ref. [4] (see also Ref. [3]) show that the morphological instability occurs (mushy zone originates) if λ_1 and T_1 are greater than the values of the order 0.15 and 1.72, respectively. This means that the latter takes place if $\lambda_1 > \lambda_{1A}$ and $T_1 > T_{1A}$. Moreover, a stable solidification scenario with the self-similar planar front is revealed in Ref. [4] for $\lambda_1 < \lambda_{1A}$ and $T_1 < T_{1A}$. From the morphological instability point of view this means that the region $\lambda_1 < \lambda_{1A}$ and $T_1 < T_{1A}$ corresponds to the stability of solidification and the region $\lambda_1 > \lambda_{1A}$ and $T_1 > T_{1A}$ characterizes another crystallization regime with a mushy zone. Strictly speaking, this domain must be described by a mushy layer model (see, for example, Ref. [4]) not by a model with the planar front without a mushy layer. Thus, the constitutional supercooling instead of instability analysis is responsible for the mushy zone incipience.

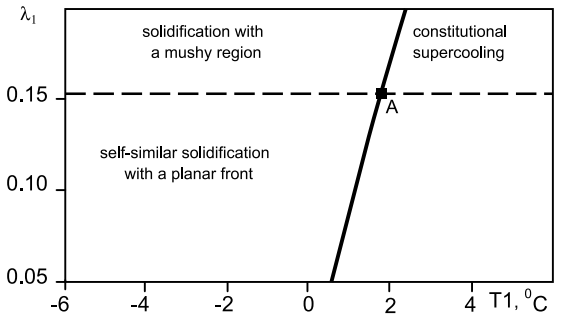

Fig. 1. The dimensionless parabolic growth rate constant λ_1 as a function of the temperature T_1 is plotted by solid curve in accordance with the self-similar solutions (14) and (15). The constitutional supercooling appears above the point A in accordance with inequality (17). Experiments [4] show that the point A is also responsible for the mushy region incipience. Thermophysical properties of the set are given in Table 1, $C_{L\infty} = 14$, $C_W = 0$, $T_{L\infty} = 15$ °C.

4. Concluding remarks

Let us summarize here the main results bearing upon our theory.

First, we show that the neutral stability curves for dynamic and morphological instabilities coincide in the case of self-similar solidification scenario or, strictly speaking, there is only one neutral stability curve in the self-similar solidification under consideration.

Secondly, the neutral stability curve and the self-similar branch of solution are not intersected for solidification, that is, a transition between stable and unstable solidification cannot be caused by the morphological instability. Thus, since experiments and numerical calculations [3] and [4] demonstrate absolute stability for two alloys before a point of constitutional supercooling, the frontal self-similar solidification regime is absolute stable before this point for all alloys in the case of any small morphological perturbations.

Thirdly, since such a transition is observed in experiments, it appears due to the influence of constitutional supercooling [3,4]. Namely, our calculations show that this transition occurs in the point of origination of the constitutional supercooling and, apparently, the latter is the reasonable criterion for the mushy zone incipience for solidification in the self-similar manner. In

Table 1
Parameter values of the set $NaNO_3 + H_2O$ used in calculations [4]

Property		Value	Units
Liquid thermal conductivity	K_L	1.3×10^{-3}	cal/(cm s °C)
Solid thermal conductivity	K_S	5.3×10^{-3}	cal/(cm s °C)
Liquid thermal diffusivity	κ_L	1.3×10^{-3}	cm^2/s
Solid thermal diffusivity	κ_S	1.2×10^{-2}	cm^2/s
Liquid diffusion coefficient	D_L	1.0×10^{-5}	cm^2/s
Solid diffusion coefficient	D_S	1.0×10^{-9}	cm^2/s
Latent heat per unit volume	L_V	73.6	cal/cm^3
Liquidus slope	m	−0.4	°C
Segregation coefficient	k	0	–

other words, if the self-similarity is established it is possible to observe the mushy zone evolution only within the framework of one of the mushy zone models and the model with the planar front without a mushy layer becomes inapplicable (see also Ref. [4]).

Of course, when the solid–liquid interface will be morphologically unstable (this occurs after the constitutional supercooling origination and the model under consideration without a mushy region is inapplicable in this case), the interface may develop in a wavy shape manner (see, for example, Ref. [3] where the picture of such a behavior is demonstrated). Further growth of the instability in the framework of a mushy zone model with the constitutional supercooling may lead to dendrites and new solid crystals nucleating ahead of the solid-mushy zone interface [3,4]. This stage of solidification was experimentally and numerically studied in details in previous works [3] and [4] and is not a subject of the present study.

Finally, apparently, the model under consideration is not quite adequate in the case of melting because the concentration distribution in the solid is a function dependent of the prehistory of solidification of an ingot and is not a function of solution. Therefore, the phase transition temperature depending on the solute distribution in the solid is also a given parameter which does not depend on an unknown concentration at the front as in the case of solidification. Therefore, the self-similar instability for melting must be studied on the basis of a model with a given solute distribution in the solid.

Acknowledgements

This work was made possible in part by award no. REC-005 of the US Civilian Research and Development Foundation for the Independent States of the Former Soviet Union (CRDF) and due to the financial support of the grants nos. 01-02-96430 Ural, 02-03-96437 Ural (Russian Foundation for Basic Research) and the grant no. E00-3.2-210 (Minobrazovanie RF). The author is grateful to the Basic Research and Higher Education Program for the financial support of young scientists.

References

[1] W.W. Mullins, R.F. Sekerka, Stability of a planar interface during directional solidification of a dilute binary alloy, J. Appl. Phys. 35 (1964) 444–451.
[2] S.R. Coriell, G.B. McFadden, R.F. Sekerka, Selection mechanisms for multiple similarity solutions for solidification and melting, J. Crystal Growth 200 (1999) 276–286.
[3] H.E. Huppert, M.G. Worster, Dynamic solidification of a binary melt, Nature 314 (1985) 703–707.
[4] M.G. Worster, Solidification of an alloy from a cooled boundary, J. Fluid Mech. 167 (1986) 481–501.
[5] D.L. Feltham, M.G. Worster, Similarity solutions describing the melting of a mushy layer, J. Crystal Growth 208 (2000) 746–756.
[6] S.R. Coriell, G.B. McFadden, R.F. Sekerka, W.J. Boettinger, Multiple similarity solutions for solidification and melting, J. Crystal Growth 191 (1998) 573–585.